ISTITUTO NAZIONALE DI FISICA NUCLEARE
Laboratori Nazionali di Frascati

LNF-77/29(R)
17 Giugno 1977

M. Piacentini: APPEARANCE POTENTIAL SPECTROSCOPY OF RARE EARTHS.

Servizio Documentazione
dei Laboratori Nazionali di Frascati
Cas. Postale 13 - Frascati (Roma)

Laboratori Nazionali Frascati
Servizio Documentazione

LNF-77/29 (R)
17 Giugno 1977

M. Piacentini(*): APPEARANCE POTENTIAL SPECTROSCOPY OF RARE EARTHS(+).

SUMMARY.

Appearance potential spectroscopy is a simple, powerful technique for studying core states as well as empty states above the Fermi surface of metals and alloys. The one-electron, one-density of states theory is derived and examples of its successes for explaining the spectra of simple metals and the 3d transition metals are discussed. Finally, it is shown that the appearance potential spectra of rare earths cannot be explained in the same way. Several other models are introduced, each of which can account only for some of the experimental features.

1. -INTRODUCTION

Appearance potential spectroscopy is an old technique, introduced in 1921 to determine the binding energy of core levels of atoms in solids[1]. Conceptually it is very simple. It consists in measuring the total yield of x-ray emission from an electron-bombarded sample. An abrupt change in the total yield is expected when the energy of the bombarding electrons reaches the binding energy of a core state, since a new channel for x-ray production is opened.

Due to the simplicity of the technique, appearance potential spectroscopy developed fast in the beginning. The onset structure was extracted from the large background emission by graphical differentiation and the binding energies of the core states of several materials were determined. But difficulties ineherent to the technique, related to sample preparation and vacuum conditions, were encountered. The number of thresholds exceeded the number of available core levels of a certain material, due to impurities. In some cases, weather conditions interfered with the experimets. However, the most serious problem was that the differentiation method was not very accurate. All these difficulties discouraged the physicists of that period and appearance potential spectroscopy was abandoned definetly in 1933, only twelve years after its birth.

In the late 1960s, appearance potential spectroscopy had its reinassence. Electronic differentiation, achieved by means of phase-sensitive techniques, allowed to extract easily the desired threshold structures from the large background. Now-a-days ultra high vacuum and sample preparation techniques do not represent anymore a problem.

The results obtained on light metals and on the 3d transition metals have been encouraging. The energy shift of a core level between a surface and a bulk atom has been measured, as well as the chemical shift due to alloying or oxidation of the material. The measured spectra could be explained using a simple one-electro model, even if in a few cases many-body effects had to be taken

(*) Gruppo Nazionale di Struttura della Materia del CNR, c/o Istituto di Fisica dell'Università, 00185 Roma, and Progetto PULS, c/o Laboratori Nazionali INFN, 00044 Frascati.

(+) This work has been the subject of a talk given by the author at the Department of Physics of the University of Messina. The author is very grateful to Prof. V. Grasso for his kind invitation. The studies on rare earths have been performed while the author was on leave at the Department of Physics of the Iowa State University, Ames, Iowa.

into account. Instead, the spectra of Ba, La and of the rare earths did not fit anymore the one--electron model. A localized, atomic picture is required.

In this note we review shortly appearance potential spectroscopy, with particular emphasis to rare earths. In sec. 2 we shall describe the experimental technique and in sec. 3 the one-electron model. In sec. 4 we shall discuss the light metals and the 3d transition metals. Sec. 5 will be devoted to the rare earth spectra.

2. - EXPERIMENTAL TECHNIQUE.

The experimental set up is sketched in Fig. 1[2, 3]. Electrons are emitted from the filament,

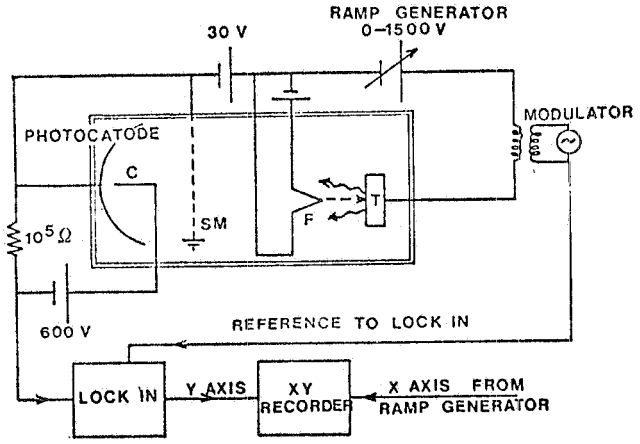

FIG. 1- Diagram of an appearance potential set-up. The devices eclosed in the large rectangle are inside an ultra high vacuum chamber. F: filament. T: target. SM: mesh grounded screen. C: collector.

usually a small, self-heated V-shaped tungsten wire, and accelerated to the sample by the accelerating voltage supplied by a ramp generator. A small modulating AC voltage is superimposed to the DC bias by means of a transformer coupled to an oscillator. The emitted x-rays reach the detector passing through a semitransparent grounded tungsten mesh. The purpose of the mesh is to avoid that the electrons emitted from the filament reach the detector region. For this reason, the filament is biased 30V positive with respect to ground. The x-rays passing the mesh strike the walls of a cilindrical tantalum photocatode, generating photoelectrons that are collected by a positively biased coaxial wire. The collector current, I_c, is a measure of the photon flux. Hereafter, we shall assume that I_c is proportional to it and, consequently, to the total yield, Y_{TOT}, of x-ray emission. The variation of the photocurrent is measured sinchronously with the AC modulating voltage using a lock-in and is directly plotted versus the accelerating voltage supplied by the ramp generator.

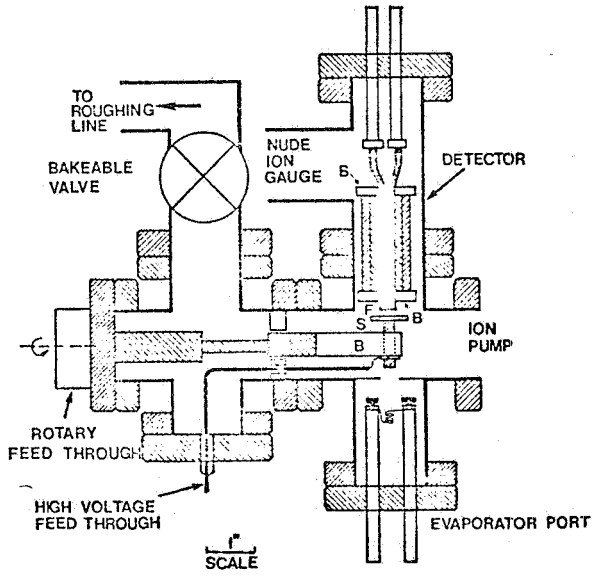

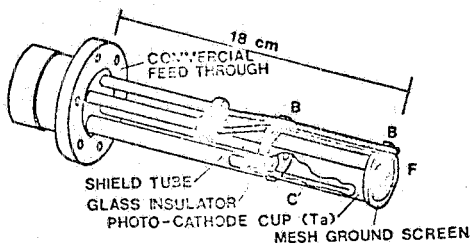

FIG. 2- Actual design of the vacuum system of an appearance potential spectrometer (ref.(3)) and of the detector mounted on a commercial 4 pin current feed through (ref. (4)). B: BN insulators: F: filament; S: sample; C: collector.

The vacuum system, shown in Fig. 2, is based on two 1 (1/2) inch crosses and one tee[3]. It permitted evaporation of samples through a baffle to keep the cathode and detector uncontaminated. Base pressures in the 10^{-11} torr were achieved. During sample evaporation the pressure could be held below 10^{-8} torr and within a few minutes later, an experimental run could be made in the 10^{-10} torr range.

The incident electron energy, E_o, is referred to the Fermi surface of the target material by:

$$E_o = eV + e\phi + 2kT \ , \tag{1}$$

where V is the applied accelerating voltage, ϕ is the work function of the filament (4.5 eV for tungsten) and 2kT is the average kinetic energy of the electrons leaving the filament at temperature T. The last two terms amount approximately to 5 eV.

The resolution of the spectrometer is affected by several contributions:

a) The voltage drop across the filament, which is of a few volts. In order to minimize this effect and to localize the emission, the tip of the V-shaped filament can be etched chemically. Another method consists in heating the filament with an AC or a pulsed current and to gate the photocurrent signal in correspondence of the zeroes of the heating current.
b) The thermal spread of the electron energy, which may amount to some tenths of eV.
c) The spread of the electron energies when the projectile electrons enter in the sample.
d) The amplitude of the modulation voltage.

There are other intrinsic factors contributing to the total width, such as the lifetime broadening of the core hole. In our experiments[2, 3], with 0.3 volts peak to peak of modulation, the sharpest features observed had a full width of about 1 eV.

3. - SIMPLE THEORY.

The total x-rays yield, $Y_{TOT}(E_o)$, contains two contributions, $Y_B(E_o)$, from the breamms-trahlung emission, and $Y_{XR}(E_o)$, from the characteristic x-rays[1, 2]:

$$Y_{TOT}(E_o) = Y_B(E_o) + Y_{XR}(E_o). \tag{2}$$

$Y_B(E_o)$ is proportional to the projectile electron enery:

$$Y_B(E_o) = C\, E_o. \tag{3}$$

The charactesitis x-rays are generated by the radiative decay of the core holes created by the incident electrons:

$$Y_{XR}(E_o) = \sum_n P_n\, \sigma_n(E_o). \tag{4}$$

P_n is the probability for the radiative decay of the core state n and it does not depend on the incident electron energy. $\sigma_n(E_o)$ is the excitation cross section of an electron in the subshell n. It is zero for energies less than the binding energy E_{bn} of the core state n, and it is a smooth function for $E_o \gg E_{bn}$. The summation into eq. 4 obviously extends over all the states with binding energies $E_{bn} < E_o$, which can be excited by the incident electron. By definition, the appearance potential spectrum $APS(E_o)$ is the first energy derivative of the total yield and, from eqs. (2), (3) and (4), is given by:

$$APS(E_o) = \frac{dY_{TOT}}{dE_o} = C + \sum_n P_n \frac{d\sigma_n}{dE_o} = C + F(E_o) + P_m \frac{d\sigma_m}{dE_o} \ . \tag{5}$$

When E_o scans across the excitation threshold energy for a certain state m, sharp structure are generated in $APS(E_o)$ only by the excitation cross section of the state m. For this reason, in the right side of eq. 5 we have separated the contribution of the newly excited state from that arising from all the other states with $E_{bn} \ll E_o \sim E_{bm}$, represented by the slowly varying function $F(E_o)$.

A direct calculation of $\sigma(E_o)$ near threshold, for low energy incident electrons, is one of the major tasks of scattering theory. Actually, it is a many-body problem, with the N electrons of the crystal and the projectile electron interacting between each other. In order to have an equation that

relates simply APS(E_o) to the crystal parameters, we use the one-electron approximation[3, 5]. Within this approximation, in the initial and final states of the N+1 electron system, all the electrons are considered not interacting with each other and the projectile electron can excite only one of the crystal electrons. From time perturbation theory, the excitation probability can be written as:

$$W_{if} = \frac{2\pi}{\hbar} \sum_{if} |\langle i | \frac{e^2}{\varepsilon |\vec{r}|} | f \rangle|^2 \; \delta(E_f - E_i). \tag{6}$$

$| i \rangle$ and $| f \rangle$ are states formed by two independent particles. $| i \rangle$ is formed by a core state wavefunction times that of a free electron of energy E_o. Since the actual state of the incident electron is not known, we must average over all such possible states. $| i \rangle$ can be assumed to be already such an average. $| f \rangle$ is an antisymmetrized wavefunction of the two electrons lying slightly above the Fermi surface (we shall take the Fermi energy E_F as the zero energy hereafter) with energies ε and ε' respectively. The interaction is the Coulomb screened potential $e^2/\varepsilon|\vec{r}|$, where $\vec{r}$ is the relative coordinate between the two electrons. Finally, the δ function in eq. (6) represents the conservation of the energy during the excitation process:

$$E_o - E_b = \varepsilon + \varepsilon' . \tag{7}$$

If in eq. (6) we neglect the variation of the matrix element (which contains the information on the type of interaction), the whole process can be described as the result of two independent transitions, as shown schematically in Fig. 3. The incident electron decays from its initial state E_o to

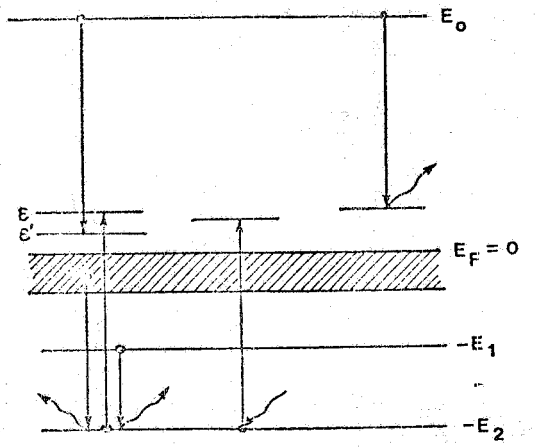

FIG. 3- Schematic diagram showing, in the one electron approximation, electron excitation of a core state (appearance potential spectroscopy)(left), soft x-ray absorption (middle), short wavelength limit of bremsstrahlung emission (right).

a final state of energy ε above E_F; the crystal electron is excited from a core state of energy E_b to a final state of energy ε' above E_F. The total transition probability is now given simply by the product of the two transition probalities, each proportional to the final density of states $N(\varepsilon)$.

$$W(E_o \longrightarrow \varepsilon \,,\; E_b \longrightarrow \varepsilon') \propto N(\varepsilon)\, N(\varepsilon'). \tag{8}$$

ε' is linked to ε by eq. (7) and it may have any value between zero, when the core electron is excited just on the Fermi surface, to a maximum value $E_o - E_b$, when it is the incident electron to rest on the Fermi surface. Each pair of values ε and ε', satisfying eq. (7) forms a possible final state for the two electron system. Thus the total yield contains a summation over all these final states:

$$Y_{XR}(E_o) \propto \int_o^{E_o - E_b} N(\varepsilon)\, N(E_o - E_b - \varepsilon)\; d\varepsilon \tag{9}$$

The interesting contribution to the appearance potential spectrum is given by:

$$APS(E_o) \approx \frac{d}{dE_o} \int_o^{E_o - E_b} N(\varepsilon) N(E_o - E_b - \varepsilon) = N(0) N(E_o - E_b) + \int_o^{E_o - E_b} \frac{dN(\varepsilon)}{d\varepsilon} N(E_o - E_b - \varepsilon) d\varepsilon . \tag{10}$$

From eq. (9), we see that the total yield is given by the self-convolution integral of the one electron density of states above the Fermi surface.

For $E_o=E_b$, eq. (10) yields $APS(E_o)=N(0)^2$, i. e. , the height of the structure above the background is proportional to the square of the density of states at the Fermi surface. If $N(\varepsilon)$ does not show sharp features, but is a smooth function of ε , $dN/d\varepsilon$ is a small quantity and the contribution from the last term into eq. (10) is negligiable. In such a case, $APS(E_o)$ is proportional to the density of final states:

$$APS(E_o) \propto N(0)\ N(E_o-E_b). \tag{11}$$

Within the frame of the one-electron approximation and constant matrix element, the soft x-ray absorption coefficient, $\alpha(\hbar\omega)$, above threshold is proportional to the density of final states. Thus we can use an experimental spectrum of $\alpha(\hbar\omega)$ inside the self-convolution integral, to obtain an expected appearance potential spectrum:

$$APS(E_o) = \frac{d}{dE_o}\int_{E_b}^{E_o} \alpha(\hbar\omega)\ \alpha(E_o+E_b-\hbar\omega)\quad d\,\hbar\omega \tag{12}$$

In a few cases, a similarity between APS and $\alpha(\hbar\omega)$ can be expected, according to eq. (11).

In Table I we present some examples of the calculated shapes of $Y_{TOT}(E_o)$ and $APS(E_o)$, obtained from model densities of states.

4. - LIGHT METALS AND 3d TRANSITION METALS.

The simple theory, giving eqs. (9) and (10), describes very well the appearance potential spectra of light metals. The appearance potential spectrum of Be[5] around the K edge shows good agreement with the calculated density of states above E_f[7] and with the soft x-ray absorption spectrum[8]. The appearance potential spectrum of Al[5,6] is presentes in Fig. 4 (full line).

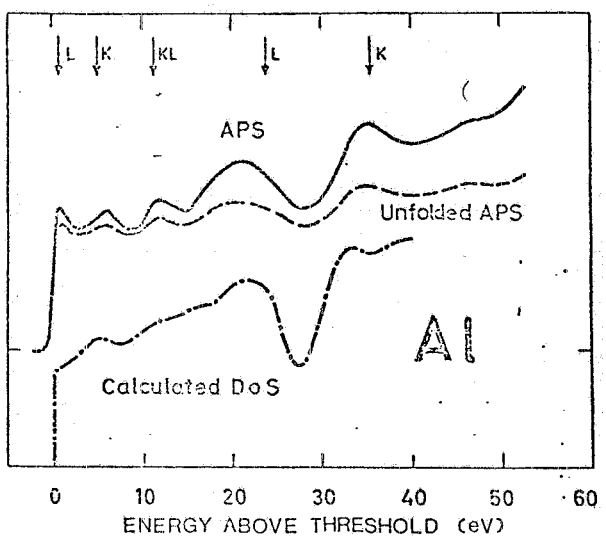

FIG. 4- (After ref.(5)) $L_{2,3}$ appearance potential spectrum of Al (full line), compared with a calculated density of states spectrum (ref. (9) - dash-dotted line)). The broken line corresponds to the density of states obtained by deconvoluting APS(E). The arrows on the top give the energies of the peaks observed in the L and in the K soft-x-ray absorption spectra of Al (ref. (9) and (10) respectively)).

The density of states obtained deconvoluting eq. (9) (broken line) differs very little from the original spectrum and agrees very well with the calculated density of states[9], indicating that the last term into eq. (10) gives only a small contribution for Al. The arrows in the upper part of Fig. 4 give the positions of the structures observed in the K and in the L soft x-ray absorption spectra[10,11]. All toghether they match the peaks observed in APS, but the two sets of arrows do not agree with each other, since the optical selection rules (given by the matrix element) allow to probe different portions of the final density of states, for different initial core levels. In the case of appearance potential spectroscopy the transition operator is the Coulomb interaction and the optical dipole selection rules are relaxed. Therefore, all the conduction density of states can be probed. This is an example

TABLE I - Calculated total yield spectra and appearance potential spectra for some model density of states in the case of metals using the one electron approximation. Energies are referred to the Fermi surface. In the left portion of the Table the analytical expressions are given. In the right portion their plots for some values of the parameters.

Constant Density of states

$N(\varepsilon) = C$

$Y(E) = \int_0^E C^2 \, d\varepsilon = C^2 E$

$dY/dE = C^2$

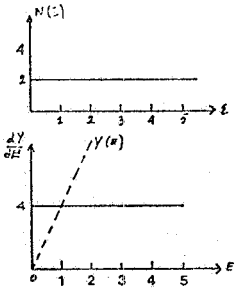

Free electron density of states

$N(\varepsilon) = \sqrt{\varepsilon + E_m}$

$Y(E) = E/2 \sqrt{E_m}\sqrt{E+E_m} + \left(\frac{E+2E_m}{2}\right)^2 \text{sen}^{-1}\left(\frac{2}{E+2E_m}\right)$

$\frac{dY}{dE} = \frac{\sqrt{E_m}}{2}\sqrt{E+E_m} + \frac{E\sqrt{E_m}}{4\sqrt{E_m+E}} + \frac{E+2E_m}{2} \text{sen}^{-1}\left(\frac{E}{E+2E_m}\right) +$

$+ \frac{(E+2E_m)\ E_m}{\sqrt{E_m+2E}}$

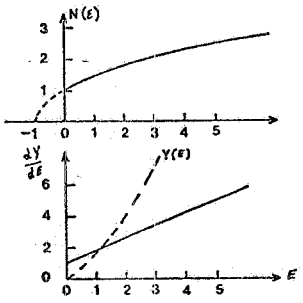

Density of states with a peak crossed by the Fermi surface

$$N(\ ) = \begin{cases} A & 0 < \varepsilon < E_1 \\ B & E_1 < \varepsilon \end{cases}$$

$$Y(E) = \begin{cases} A^2E & 0 < E < E_1 \\ (2AB - A^2)E + 2A(A-B)E_1 & E_1 < E < 2E_1 \\ B^2E + 2B(A-B)E_1 & 2E_1 < E \end{cases}$$

$$\frac{dY}{dE} = \begin{cases} A^2 & 0 < E < E_1 \\ 2AB - A^2 & E_1 < E < 2E_1 \\ B^2 & 2E_1 < E \end{cases}$$

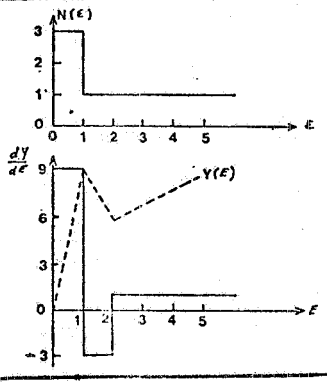

Density of states with a peak above the Fermi surface

$$N(\varepsilon) = \begin{cases} B & 0 < \varepsilon < E_1 \\ A & E_1 < \varepsilon < E_2 \\ B & E_2 < \varepsilon \end{cases}$$

$$Y(E) = \begin{cases} B^2E & 0 < E < E_1 \\ -2B(A-B)E_1 + B(2A-B)E & E_1 < E < E_2 \\ B^2E + 2B(A-B)(E_2-E_1) & E_2 < E < 2E_1 \\ \left[(A-B)^2+B^2\right]E + 2(A-B)(BE_2 - AE_1) & 2E_1 < E < E_1+E_2 \\ A(2B-A)E + 2(A-B)(AE_2 - BE_1) & E_1+E_2 < E < 2E_2 \\ B^2E + B(E_2-E_1)(2A-B) & 2E_2 < E \end{cases}$$

$$\frac{dY}{dE} = \begin{cases} B^2 & 0 < E < E_1 \\ B(2A-B) & E_1 < E < E_2 \\ B^2 & E_2 < E < 2E_1 \\ (A-B)^2+B^2 & 2E_1 < E < E_1+E_2 \\ A(2B-A) & E_1+E_2 < E < 2E_2 \\ B^2 & 2E_2 < E \end{cases}$$

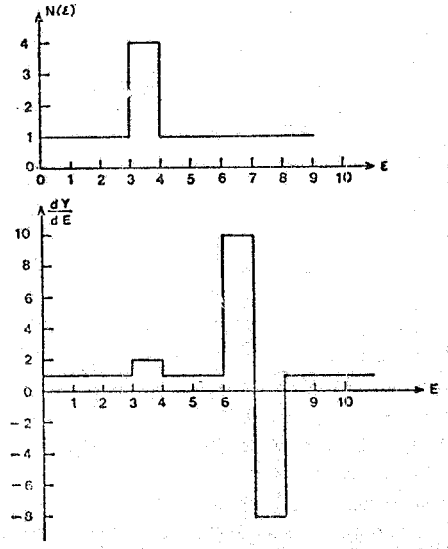

of how appearance potential spectroscopy is more powerful than optical techniques to study the empty states above E_F.

The 3d transition metals Mn to Ni form a second class of materials extensively studied (see refs. 1, 6, 12, 13, 14). The conduction density of states can be represented simply by a peak generated by the 3d states superimposed to the smooth s-p free-electron like band. The Fermi surface lies in between the d bands and moves upwards for increasing atomic number Z . We can picture this situation with the third example of Table I. The expected appearance potential spectra should consist of a positive peak of width E_1, corresponding to the width of the unfilled portion of the d--bands, followed by a dip. The intensity of the peak should be proportional to the square of the density of states at the Fermi surface. The reduction of the dip with respect to the positive peak height measures the relative contribution of the s-p states to the total density of states.

The $L_{2,3}$ appearance potential spectra of the 3d transition metals [5, 12, 13] confirm the previous expectations. The sepctra consist of a doublet, corresponding to the spin-orbit splitting of the 2p level. Each component consists of a peak, followed by the negative dip. In Fig. 5 the appearance potential spectrum of Cr is shown and compared with a calculated spectrum[3] obtained from eq. (12), using the $L_{2,3}$ soft-x-ray absorption spectrum by Fisher[15]. The agreement is very good, except for a slight shift of the calculated spectrum to higher energies. This shift is caused by the fact that appearance potential spectroscopy probes surface atoms only, while the soft x-ray absorption probes bulk properties. The binding energies of core states of atoms lying on the surface is reduced with respect to the bulk ones because of the smaller coordination and the smaller screenening from the conduction electrons (see ref. (16)). As a matter of fact, tha binding energies obtained from appearance potential spectroscopy resulted lower than those measured with other techniques (ESCA and x-ray emission)[16]. In Fig. 6 the appearance potential spectrum of Ni is shown[6]. The L_3 line width is much narrower than that of Cr and the dip is almost missing indicating the larger contribution to the total density of states given by the s-p bands in the present case.

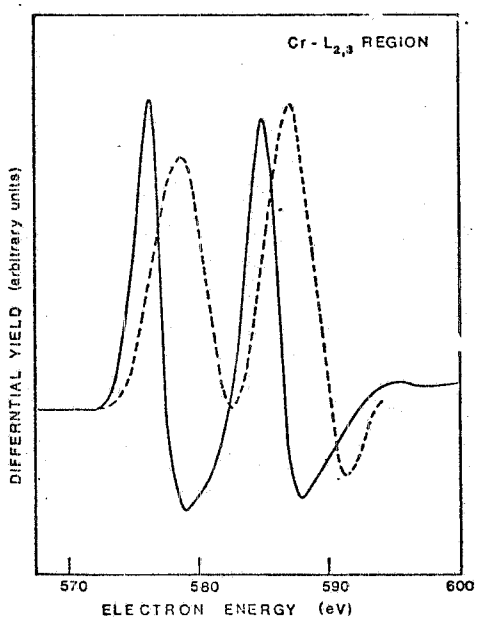

FIG. 5- $L_{2,3}$ appearance potential spectrum of Cr (ref. (12)) compared with the self convalution spectrum of the $L_{2,3}$ soft x-ray absorption spectrum (ref. (15)) calculated according to eq. (12).

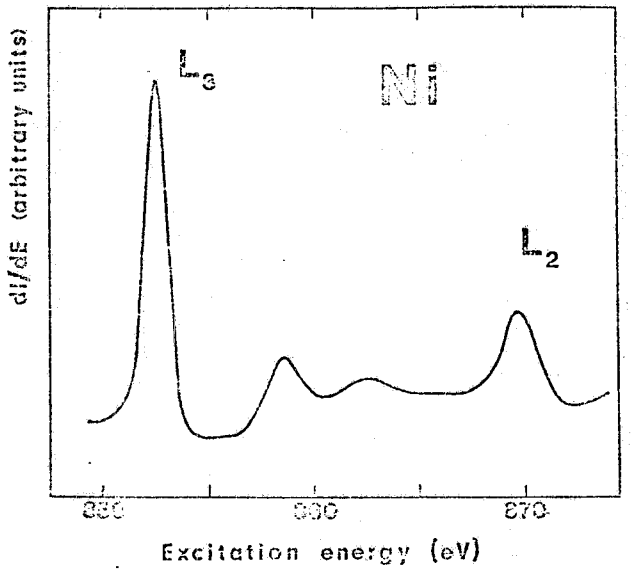

FIG. 6- $L_{2,3}$ appearance potential spectrum of Ni, from ref. (6).

In Fig. 7 the L_3 line width is plotted for increasing Z[12]. As expected E_1 decreases and it agrees well with calculated values[17], if account is made also for the lifetime broadening.

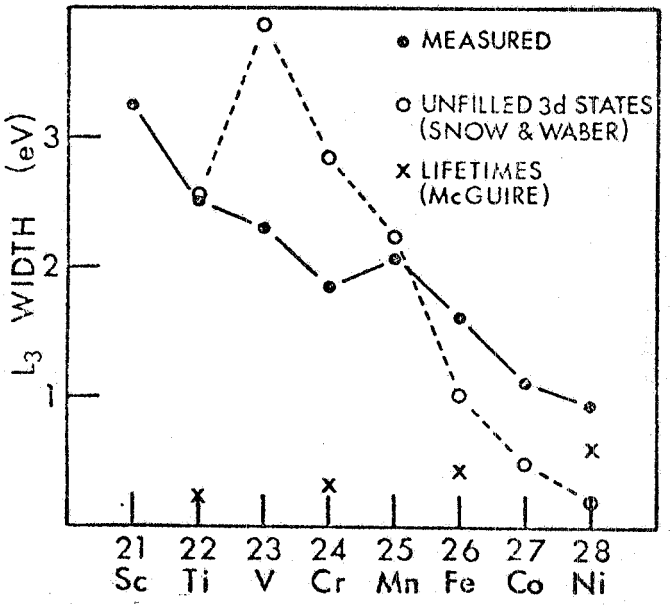

FIG. 7- (From ref. (12)) L_3 peak widths of the 3d transition metals, measured at half maximum and corrected for 1 eV instrument response function (solid dots), compared with those calculated by Snow and Waber[17] for the width of the unifilled 3d band (open circles) and L_3 lifetimes calculated by McGuire (X's) (unpublished).

Of particular interest may be the application of appearance potential spectroscopy to alloy problems. Ertl and Wandel[18] showed that the appearance potential spectra of a Ni/Cu alloy in the Ni $L_{2,3}$ thereshold region, cannot be described by the rigid band-model, according to which at 55% concentration of Cu, the Ni d-bands should be completely filled and the peaked structure should disappear. From the analysis of the intensity of the L_3 line as a function of the concentration, they concluded also that the improved CPA model describes adequately the properties of the Cu/Ni alloy.

5. - APPEARANCE POTENTIAL SPECTROSCOPY OF RARE EARTHS.

The density of conduction states above E_F for rare earths should be similar to that of the 3d transition metals, consisting of a strong peak of density of states, originating from the empty 4f levels, crossed by the Fermi level. Thus one should expect small differences with respect to the transition metals. The appearance potential spectrum of La between 0 and 1300 eV is shown in Fig. 8[2]. The vertical bars indicate the threshold energies for exciting core states[19]. Structure clearly appears in correspondence of the n=3 (M) and n=4 (N) subshells.

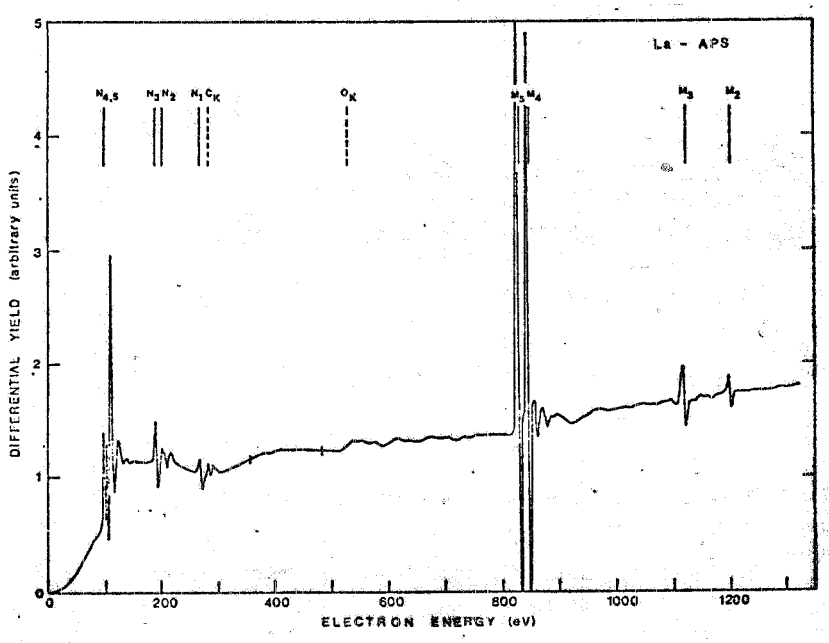

FIG. 8 - Apperance potential spectrum of La from 0 to 1300 eV[2]. The vertical lines mark the atomic core binding energies (ref. (19)).

The excitation of the 3d and 4d levels generate the strongest features. The spin orbit splittings of the 3p, 3d and 4p states are well resolved, but not that of the 4d levels. The $M_{4,5}$ structure are so strong to show up clearly as peaks even in the total yield spectra. Remarkable differences occurred between clean and contaminated (oxidized) samples: in the latter case the chemical shift, broadening and fewer features were observed. This is particularly interesting for the $M_{4,5}$ region where soft x-ray absorption did not show any difference[20].

However, the appearance potential spectra of rare earths strongly differ from those of the 3d transition metals and deviate from the simple theory eq. (10)[21, 22, 23]. In particular, the $N_{4,5}$ spectrum, shown for La in Fig. 9[23], shows more structures than the two spin orbit components.

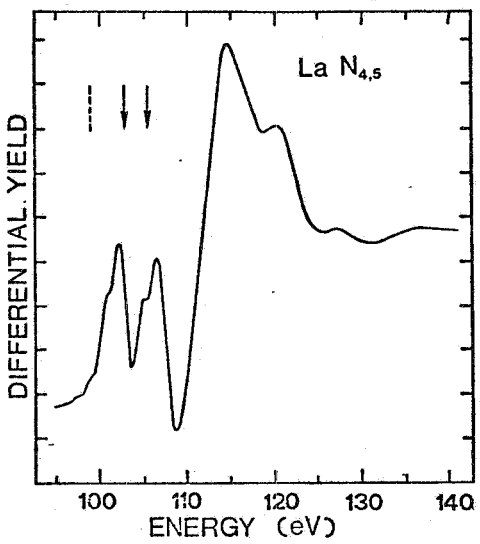

FIG. 9 - La $N_{4,5}$ appearance potential spectrum (ref. (2,23)). The two arrows mark the energies for exciting $4d_{3/2,\,5/2}$ electrons to E_F (ref. (24)). The dashed arrow corresponds to the binding energy of the 4d states (ref. (19)).

Second, structure appears at energies lower than the threshold energy indicated by the lines in the upper part of Fig. 9[19, 24]. Third, eq. 12 yielded a spectrum which is totally different from the measured one[2, 23].

A first clue in understanding the appearance potential spectra of rare earths is given by the $N_{4,5}$ soft-X-ray absorption spectra. These spectra show several weak, very sharp lines below the expected 4d excitation threshold and a very broad band, some 10 eV wide, above threshold[25, 26, 27]. A one-to-one correspondence between optical structures and appearance potential structures can be found, as shown in Table II[2]. An empirical rule can be derived too, that for transitions whose final states lie below the ionization threshold, the appearance potential peaks are shifted by a constant amount to higher energies than the corresponding optical peaks. Dehemer et al.[28-31] explained the soft x-ray absorption spectra in terms of atomic-like transitions. Most of the oscillator strength for exciting a 4d electron goes into the transitions $4d^{10}\,4f^N \rightarrow 4d^9\,4f^{N+1}$ (N=0 for La and N=13 for Lu). The wavefunction of the excited electron is localized well inside the centrifugal barrier and strongly overlaps the 4d wavefunctions. The exchange interaction between the 4d hole and the 4f electron splits the $4d^9\,4f^{N+1}$ configuration into a multiplet spread over 20 eV. Some of the levels remain below the ionization threshold, generating the sharp lines observed experimentally, while the others are pushed in the continuum and are broadened by autoionization. These are the strongest structure, generating the broad band in the optical spectra. Calculations performed on several triply ionized rare earth ions[28, 29, 30, 31] gave the energies and the oscillator strengths of the lines in good agreement with experiment[25, 26, 27]. To support this atomic explanation, the spectra of the rare earth metals[25-27], rare earth compounds[32] and of isolated atoms[33] agree with each other. The same explanation holds for the excitation of the 3d states[20, 34]. But in this case the exchange interaction is smaller than the spin-orbit interaction and the lines are grouped around the two spin-orbit components.

The excitation process is definetly atomic-like and the simple theory, eqs. (9) and (10), cannot be expected to work. In order to construct a new model to explain the appearance potential spectra of rare earths, we shall proceed as follows.

TABLE II - Energies (in eV) of the structures observed in the $N_{4,5}$ soft x-ray absorption spectra $\alpha(\hbar\omega)$ (first column) and of the $N_{4,5}$ appearance potential spectra (second column) of La and Ce. In the third column the type of structure observed in APS(E) is indicated. The energy differences between features in APS(E) and the corresponding ones in $\alpha(\hbar\omega)$ are given.

LANTHANUM				CERIUM			
$\alpha(\hbar\omega)$	APS	Type of structure	ΔE	$\alpha(\hbar\omega)$	APS	Type of structure	ΔE
					100.7	step	
	97.2	step	0	101.3	103.2	peak	1.9
97.2	101.4	shoulder	4.2	103.5	105.0	peak	1.5
	102.7	peak	5.5	104.6	104.3	shoulder	1.7
	105.5	peak	4.1	105.8	107.2	peak	1.4
101.3	106.9	peak	5.6	106.1			
				106.6	108.2	shoulder	1.6
				108.1	110.0	peak	1.9
				108.9			
				109.7			
				110.4	112.6	peak	2.2
				111.5	113.7	shoulder	2.2

In sec. 3 the scattering process was ultimately approxiamated with two transitions performed indipendently by the incident and core electrons respectively. In this case, the total transition probability is given by the product of the two transition probabilities. It was straight forward to use same density of final states for both electrons, which is correct for nearly free electron bands. Instead, a more careful analysis is required in the case of localized excitations.

If we look again at the two transition, sketched in the diagram of Fig. 3, we see that the projectile electron undergoes the same process which gives rise to the short wavelength limit of the bremsstrahlung spectrum. After scattering, it moves freely through the crystal, probing the "true" density of states. The core electron performs a transition to an excited state of the crystal, such as in the soft x-ray absorption. The excited state may be either free-electron like or localized. The former case gives the one electron-one density of states model discussed in sec. 3. In the latter case $\alpha(\hbar\omega)$ may depend on a "localized" density of states or on matrix element effects, and it differs from $N(\varepsilon)$, as it is shown in Fig. 10, where the bremsstrahlung short wavelength limit[35] and

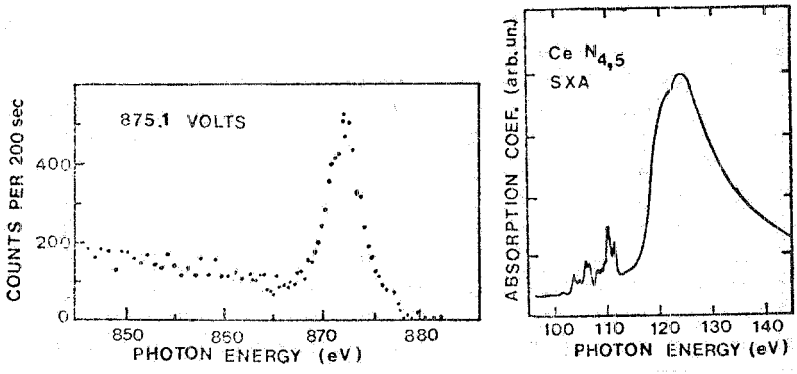

FIG. 10 - Soft x-ray $N_{4,5}$ absorption spectrum of Ce (ref. (27)-right), compared with the bremsstrahlung short wavelength continuum edge (ref. (35)- left).

the $N_{4,5}$ soft x-ray absorption spectrum of Ce[27] are shown. Nevertheless, $\alpha(\hbar\omega)$ in still representative of the core elecron transition probability. In this way we arrive to the two-density of states model proposed by Wendin for explaining the appearance potential spectrum of Ba[36]. Eq. (10) is replaced by:

$$APS(E_o) \propto \omega \frac{d}{dE_o} \int_o^{E_o - E_b} N(\varepsilon)\alpha(\hbar\omega - \varepsilon)\, d\varepsilon \qquad (13)$$

We applied eq. (13) to the $N_{4,5}$ spectra of La and Ce, using the isochromat spectra of Liefeld et al. (see ref. (37)) for La and of Chamberlain et al.[35] for Ce and the soft x-ray absorption data of Haensel et al.[27]. The main structure are reproduced, as shown in Fig. 11 for La and Fig. 12 for Ce.

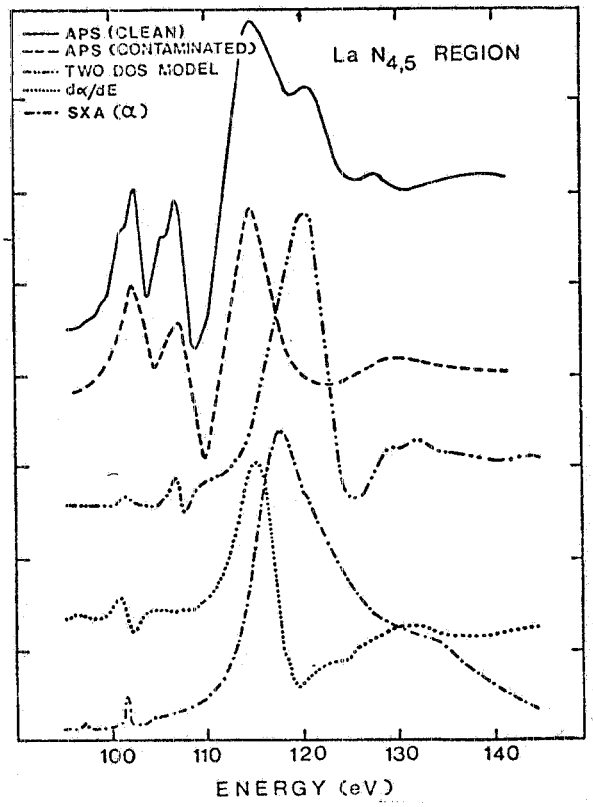

FIG. 11 - $N_{4,5}$ appearance potential spectrum of La compared with several calculated model spectra. — APS(E) of a clean sample; – – – APS(E) of a contaminated sample; – ·· – ·· two density of states model calculation; — · — · soft x-ray absorption spectrum; · · · · energy derivative of the soft x-ray absorption spectrum.

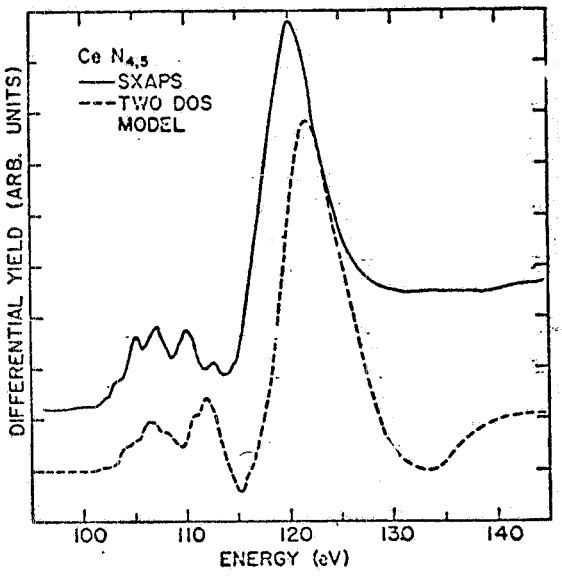

FIG. 12 - $N_{4,5}$ appearance potential spectrum of Ce (full line), compared with the calculated two density of states curve (broken line) (ref. (2)).

Now we are able to understand what is occurring.

When one of the atomic-like excited states is reached, the final energy for the core electron is fixed and the total yield becomes proportional to the crystal density of states. This derives immediately from eq. (13), by representing the absorption line with a δ function ($\alpha(\hbar\omega) \propto \delta(\hbar\omega - E_n)$). Thus, a step-like structure is expected in correspondence of the soft x-ray absorption line, followed at higher energies by a peaked structure, associated with the peak of the bremsstrahlung isochromat spectrum. Indeed, this is found in the case of the $N_{4,5}$ spectra of La and Ce, as shown in Table II. Unfortunately the steps corresponding to the higher excited lines could not be resolved in our $APS(E_o)$ spectra. The $N_{4,5}$ spectrum of La shows several other features which do not fit in either of the previous models. The structure at 117 eV, as well as all the spectrum of the contaminated sample up to about 135 eV, is reproduced fairly well by the spectrum of $d\alpha(\hbar\omega)/d\hbar\omega$, as it can be seen in Fig. 11. No

satisfactory explanation has been found yet for the splitting into two components separated by 1.3 eV, of the two features around 102 and 107 eV, observed in going from the contaminated to the clean material.

The $M_{4,5}$ appearance potential spectra, shown in Fig. 13 for La and Ce[2], require another approach. The two density of states model can explain a few of the experimental features. For istance, in La the three thresholds at 830, 834 and 850 eV occur at the same energies as the three soft x-ray

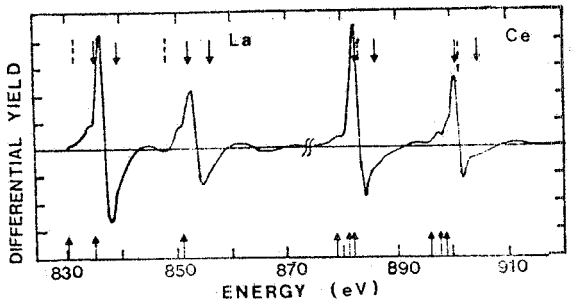

FIG. 13 - $M_{4,5}$ appearance potential spectra of clean La and Ce (ref. (2)). The dashed lines are binding energies (ref. 19)); the upper arrows are x-ray photoemission peak positions (ref. (24)) and the lower arrows mark soft x-ray absorption peak positions (ref. (20)).

absorption lines, indicating the onset of their excitation. But the two strong, dispersion like features crossing zero at 837.5 and 854 eV respectively, are due to a completely different phenomenon. In fact, in La and Ce the peak a few eV above the bremsstrahlung continuum threshold, due to the preferential scattering of the incident electrons into empty 4f states, is strongly enhanced when E_0 exceeds slightly the excitation energy of a 3d electron[35, 37]. $M_{4,5}$ appearance potential structures can be accounted for by integrating the series of isochromat spectra measured by ref. (35) and (37) and differentiating them with respect to the incident electron energy[22]. The following mechanism for the observed enhancement has been proposed[35, 36, 37]. A negative ion bound state is formed temporarily with both the projectile electron and the excited electron in a 4f state on the same rare earth atom. Then, this state decays with one of the electrons filling the 3d hole and the other electron occupying a vacant 4f state. The final state of the system does not differ from that obtained by a direct bremsstrahlung process. Since the intermediate state is only virtual, the emitted x-rays are monochromatic, while the normal decay of a 3d hole generates the characteristic x-ray spectrum, with the emission of the $M_{4,5}$ as well as of all the other possible lines. To support this picture, the $M_{4,5}$ appearance potential spectrum of Sm showed a decrease of the characteristic x-ray line with respect to the resonant line when measured with an Al filter[38].

6. - CONCLUSIONS.

In this review, we have discussed briefly a few problems connected with appearance potential spectroscopy. In the case of light metals and the 3d transition metals, the one-electron-one-density of states model works well. The full potentiality of appearance potential spectroscopy to measure core binding energies, and their shifts for surface atoms with respect to bulk atoms, or due to different chemical enviroments, has been shown. It is also a very useful and simple technique to probe the conduction density of states.

When localized, atomic-like excitations occur as for the 3d and 4d electrons of rare earths, the previous model fails and different approaches are required. We have suggested here a two density of states model, which can explain only a part of the observed features. A resonance of the bremsstrahlung continuum is also suggested for some structures. To arrive to a unified model for the case of rare earths is still necessary a great effort both theoretical and experimental.

REFERENCES

(1) - For a short history of the appearance potential spectroscopy see, for istance, the review paper: R. L. Park and J. E. Houston, J. Vac. Sci. Technol. 11, 1 (1974).
(2) - R. J. Smith, M. Piacentini, J. L. Wolf and D. W. Lynch, Phys. Rev. B14, 3419(1976).
(3) - R. J. Smith, PhD Thesis, Iowa State University 1975 (unpublished).
(4) - R. G. Musket and S. W. Taatjes, J. Vac. Sci. Technol. 9, 1041 (1971).
(5) - P. O. Nilsson and J. Kanski, Surface Science 37, 700 (1973).
(6) - J. Kanski, PhD Thesis, Chalmers Tekniska Hogskola, Gotebors 1974, (unpublished)
(7) - P. O. Nilsson, G. Arbman and T. Gustafsson, J. Phys. F4, (1974).
(8) - R. W. Johnston and D. H. Tomboulian, Phys. Rev. 94, 1585(1954).
(9) - J. W. D. Connolly, Int. J. Quantum Chem. IIs, 807, (1970).
(10) - R. Haensel, G. Keitel, B. Sonntag, C. Kunz and P. Schreiber, Phys. Stat. Solidi a2, 85(1970).
(11) - R. J. Liefeld, Soft x-ray Band Spectra (ed. D. J. Fabian) (Academic Press, 1968).
(12) - R. L. Park and J. E. Houston, Phys. Rev. B6, 1073 (1972).
(13) - J. E. Houston and R. L. Park, Electron Spectroscopy (Ed. D. A. Shirley) (North Holland, 1972), pag. 895.
(14) - J.E. Houston and R. L. Park, J. Vac. Sci. Techol. 9, 579 (1972).
(15) - D. W. Fisher, Phys. Rev. B4, 1778 (1971).
(16) - J. E. Houston, R. L. Park and G. E. Laramore, Phys. Rev. Letters 30, 846 (1973).
(17) - E. C. Snow and J. T. Waber, Acta Met. 17, 623 (1969).
(18) - G. Ertl and K. Wandelt, Phys. Rev. Letters 29, 218 (1972).
(19) - J. A. Bearden and A. F. Burr, Rev. Mod. Phys. 39, 125 (1967).
(20) - C. Bonnelle, R. C. Karnatak and J. Sugar, Phys. Rev. A9, 1920 (1974).
(21) - Deviations from the one electron theory, eq. (9), were observed previously in the appearance potential spectrum of Ba, see e. g. J. Kanski and P. O. Nilsson, Phys. Letters 45A, 399 (1973).
(22) - W. E. Harte, P. S. Szczepanek and A. J. Leyendecker, Phys. Rev. Letters 33, 86 (1974).
(23) - R. Smith, M. Piacentini and D. W. Lynch, Phys. Rev. Letters 34, 476 (1975).
(24) - I. Nagakura, T. Ishii and T. Sagawa, J. Phys. Soc. Japan 33, 754 (1972).
(25) - T. V. Zimkina, V. A. Fomichev, S. A. Gribovskii and I. I. Zhukova, Fiz. Tverd. Tela 9, 1447 (1967) (Soviet Phys. -Solid State 9, 1128).
(26) - V. A. Fomichev, T. M. Zimkina, S. A. Gribovskii, and I. I. Zhukova, Fiz. Tverd. Tela 9, 1490 (1967) (Soviet Phys. -Solid State 9, 1163).
(27) - R. Haensel, P. Rabe and B. Sonntag, Solid State Commun. 8, 1845 (1970).
(28) - J. L. Dehmer, A. F. Starace, U. Fano, J. Sugar and J. W. Cooper, Phys. Rev. Letters 26, 1521(1971).
(29) - A. F. Starace, Phys. Rev. B5, 1773 (1972).
(30) - J. Sugar, Phys. Rev. B5, 1785 (1972).
(31) - J. L. Dehmer and A. F. Starace, Phys. Rev. B5, 1792 (1972).
(32) - D. W. Lynch and C. G. Olson, Proc. Intern. Conf. Vacuum Ultraviolet Radiation Physics, Hamburg 1974 (Vieweg Pergamon, 1974), p. 258.
(33) - H. W. Wolff, R. Bruhn, K. Radler and B. Sonntag, Report Desy SR-76/14(1976).
(34) - J. Sugar, Phys. Rev. A6, 1764 (1972).
(35) - M. B. Chamberlain, A. F. Burr and R. J. Liefeld, Phys. Rev. A9, 663 (1974).
(36) - G. Wendin, Proc. Intern. Conf. Vacuum Ultraviolet Radiation Physics, Hamburg 1974 (Vieweg Pergamon, 1974), p. 252.
(37) - R. L. Liefeld, A. F. Burr and M. B. Chamberlain, Phys. Rev. A9, 316 (1974).
(38) - M. B. Chamberlain and W. L. Baun, J. Vac. Sci. Technol. 11, 441 (1974).